



# One-step synthesis of nonstoichiometric TiO<sub>2</sub> with designed (101) facets for enhanced photocatalytic H<sub>2</sub> evolution



Wei-Kang Wang<sup>a</sup>, Miao Gao<sup>a</sup>, Xing Zhang<sup>a</sup>, Mamoru Fujitsuka<sup>b</sup>, Tetsuro Majima<sup>b,\*</sup>, Han-Qing Yu<sup>a,\*</sup>

<sup>a</sup> CAS Key Laboratory of Urban Pollutant Conversion, Department of Chemistry, University of Science & Technology of China, Hefei, 230026, China

<sup>b</sup> The Institute of Scientific and Industrial Research (SANKEN), Osaka University, Mihogaoka 8-1, Ibaraki, Osaka 567-0047, Japan

## ARTICLE INFO

### Article history:

Received 15 October 2016

Received in revised form 8 December 2016

Accepted 11 December 2016

Available online 12 December 2016

### Keywords:

Self-doping

Facet etching

Photocatalytic reduction

Charge transfer dynamics

## ABSTRACT

Photocatalyst is widely applied in environmental remediation and energy conversion. Appropriately engineered band structures of semiconductor photocatalysts are beneficial for enhancing surface reactions under light irradiation. Exposing the highly reductive facets of TiO<sub>2</sub> crystals has been recognized as an efficient approach to promote photocatalytic reduction reaction. However, there is no report about the application of one-step solvothermal reaction for the synthesis of the TiO<sub>2</sub> crystals with (101) facets and in-situ doping. In this work, non-stoichiometric anatase TiO<sub>2</sub> microspheres with designed (101) facets were successfully synthesized by using one-step solvothermal reaction. The prepared non-stoichiometric anatase TiO<sub>2</sub> microspheres with designed (101) facets exhibited a great photocatalytic activity for H<sub>2</sub> evolution with a reaction rate of 3.4 times faster than that of anatase TiO<sub>2</sub> that was neither etched nor doped. The (101) facets of anatase TiO<sub>2</sub> were found to be able to generate and transmit more reductive electrons to promote the H<sub>2</sub> evolution in the photocatalytic reduction reaction. With the femtosecond time-resolved diffused reflectance measurement, the roles of self-doping Ti<sup>3+</sup> as the photogenerated electrons trapping and (101) facets were further elucidated. Our findings might provide a new opportunity to develop an efficient, cost-effective and promising TiO<sub>2</sub>-based catalyst for enhanced photocatalytic H<sub>2</sub> production.

© 2016 Published by Elsevier B.V.

## 1. Introduction

Photocatalysis is an environmentally friendly process for environmental remediation and energy conversion [1]. Titania has been recognized as one of the most promising and suitable photocatalytic materials due to its abundant availability, nontoxicity, and high chemical stability [2]. In principle TiO<sub>2</sub> is an ideal photocatalyst. However, since photoinduced electron-hole pairs of anatase TiO<sub>2</sub> are easy to recombine, resulting in their lower photocatalytic activity, the capability to efficiently separate photoinduced electron-hole pairs needs substantial improvement [3]. So far, various approaches have been explored to improve the photocatalytic activity of TiO<sub>2</sub>.

Crystal facet is one of the most significant factors governing the photocatalytic performance of TiO<sub>2</sub> [4–6]. Some recent studies have demonstrated that the crystal facets play a critical role in improving photocatalytic activity of TiO<sub>2</sub> [7]. A new “surface

heterojunction” concept was proposed based on the density functional theory calculations to highlight the effect of crystal facets on the photosynthetic activity of TiO<sub>2</sub> as a result of the transfer of photogenerated electrons and holes to (101) and (001) facets, respectively [8]. Single-molecule imaging and kinetic analysis of the fluorescence have further confirmed reaction sites by detecting reduced probe molecules located on the (101) facets, rather than the (001) facets of TiO<sub>2</sub> [9]. Meanwhile, strong evidence of charge separation on anatase TiO<sub>2</sub> crystals with selectively etched (001) facets was reported [10]. In this case, the appropriate corrosion on (001) facets could facilitate electron-hole separation and transfer. Moreover, various experiments have shown that the (101) facets of TiO<sub>2</sub> with a higher thermodynamic stability exhibit a higher reactivity than the (001) facets in photocatalytic H<sub>2</sub> evolution [11,12].

Recently, it has been reported that the reduced Ti<sup>3+</sup>-containing TiO<sub>2</sub> (TiO<sub>2-x</sub>), creates localized oxygen vacancy states, which are beneficial for the electron mobility [13]. Compared to the conventional doping, oxygen vacancy is facile self-doping without inducing any impurity elements. To date, several methods have been developed to synthesize the reduced TiO<sub>2</sub> with improved photocatalytic performance. For instance, a metallic zinc-assisted

\* Corresponding authors.

E-mail addresses: [majima@sanken.osaka-u.jp](mailto:majima@sanken.osaka-u.jp) (T. Majima), [hqyu@ustc.edu.cn](mailto:hqyu@ustc.edu.cn) (H.-Q. Yu).

method has been used to synthesize  $\text{Ti}^{3+}$  doped  $\text{TiO}_{2-x}$  [14]. Some other methods such as plasma treatment [15], laser irradiation [16], or high-energy particle bombardment [17] have also been used to achieve the doping of  $\text{Ti}^{3+}$  into  $\text{TiO}_{2-x}$ . Although substantial progress on facet and doping has been made in preparing  $\text{TiO}_2$ -based materials, exploration of one-step method to achieve in-situ  $\text{Ti}^{3+}$  self-doping  $\text{TiO}_2$  with designed (101) facets for enhanced photocatalytic  $\text{H}_2$  evolution is highly desired.

In this work, non-stoichiometric anatase  $\text{TiO}_2$  microspheres with designed (101) facets were synthesized using a simple solvothermal method. Two strategies of facet-etching and doping were adopted to improve the photocatalytic reduction capacity of  $\text{TiO}_2$  microspheres. Furthermore, the prepared non-stoichiometric anatase  $\text{TiO}_2$  microspheres with (101) facets were used to produce  $\text{H}_2$  under UV light irradiation to examine whether the facet etching and  $\text{Ti}^{3+}$  self-doping enhance its photocatalytic activity. The mechanisms behind the effects of self-doping  $\text{Ti}^{3+}$  as the photogenerated electrons trapping and (101) facets were further elucidated using the femtosecond time-resolved diffused reflectance (TDR) measurement.

## 2. Materials and methods

### 2.1. Sample preparation

All chemicals used in this work were analytical-grade reagents and used without further purification. The  $\text{Ti}^{3+}$  solution was synthesized following the method reported previously [18,19]. Briefly, 0.15 g of  $\text{NH}_4\text{F}$  was dissolved in 15 mL of  $\text{Ti}^{3+}$  solution in 50 mL of beaker. After 15-min stirring, 25 mL of ethanol was added to the mixed solution. After additional 15-min stirring, the solution was transferred into a polytetrafluoroethylene (Teflon)-lined stainless autoclave with a total volume of 50 mL. The solvothermal synthesis was carried out at  $160^\circ\text{C}$  for 4 h (denoted  $\text{TiO}_2$ -1) and 12 h (denoted  $\text{TiO}_2$ -2) in an electric oven respectively. The autoclave was cooled to room temperature after the growth process. Then, the obtained samples were ultrasonically cleaned using ethanol and water in sequence. Before the photocatalytic properties were measured, all the samples were treated with  $\text{NaOH}$  (0.1 M) to remove the adsorbed fluorine ions. The third sample ( $\text{TiO}_2$ -3) was obtained by annealing the sample ( $\text{TiO}_2$ -2) at  $500^\circ\text{C}$  for 4 h.

To prepare  $\text{Pt/TiO}_2$  composites, the catalyst (2 mg) and  $\text{H}_2\text{PtCl}_6 \cdot 6\text{H}_2\text{O}$  (0.02 mg of Pt) were dispersed into an aqueous methanol solution (1 mL of  $\text{CH}_3\text{OH}$  and 4 mL of  $\text{H}_2\text{O}$ ) in a glass tube. The mixture was under irradiation (UV light 365 nm) with magnetic stirring for half an hour. Then, the Pt-loaded  $\text{TiO}_2$  samples were cleaned with water.

### 2.2. Catalyst characterization

The X-ray diffraction (XRD) patterns of the samples were obtained by a diffractometer (TTR-III, Rigaku Co., Japan) using  $\text{Cu K}\alpha$  radiation source ( $\lambda = 1.541841 \text{ \AA}$ ) at a scan speed of  $8^\circ/\text{min}$  to determine the crystal phase of the obtained samples. The accelerating voltage and the applied current were 40 kV and 200 mA, respectively. The morphology and microstructure of the  $\text{TiO}_2$  nanostructures were characterized by field-emission scanning electron microscope (SEM, SIRION200, FEI Co., USA). The morphology and structure were characterized with a transmission electron microscope (TEM, JEM2100, JEOL Co., Japan). High-resolution transmission electron microscopy (HRTEM) images were obtained on a transmission electron microscope (JEM-2010, JEOL Co., Japan) with an accelerating voltage of 200 kV. The low temperature electron paramagnetic resonance (EPR) spectra of the samples were recorded at 150 K to confirm the presence of  $\text{Ti}^{3+}$  (JES-FA200, JEOL

Co., Japan) (140 K, 9064 MHz, 0.998 mW, X-band). The  $g$  values were determined using a 2,2-diphenyl-1-picrylhydrazyl (DPPH) standard. The optical absorbance spectra of the samples were obtained using a UV-vis spectrophotometer (SOLID3700, Shimadzu Co., Japan). X-ray photoelectron spectroscopy (XPS) analysis was conducted to investigate the chemical state of samples (PHI 5600 XPS spectroscopy, Ulvac-Phi Co., Japan). The measurement of surface area was conducted using the Brunauer-Emmett-Teller (BET) method on TriStar II 3020 V1.03 (Micromeritics Instrument Co., USA).

### 2.3. Photoelectrochemical measurements

Electrochemical measurements were all performed on an electrochemical station (ALS CH 660B, CH Instruments Inc., USA). The transient photocurrent and electrochemical impedance spectroscopy (EIS) were measured in a homemade three-electrode system, in which commercial glassy carbon electrode (GC, an effective area of  $0.071 \text{ cm}^2$ ) deposited with  $\text{TiO}_2$  samples was used as the working electrode, Pt wire as the counter electrode, and  $\text{Ag/AgCl}$  as the reference electrode. To determine the charge-transfer resistance at the electrode/electrolyte interface, EIS analysis was conducted at an open-circuit potential (OCP) by applying an AC voltage amplitude of 5 mV within the frequency range from  $10^5$  to  $10^{-2} \text{ Hz}$  in 0.2 M  $\text{Na}_2\text{SO}_4$  solution.

### 2.4. Photocatalytic measurements

Photocatalytic  $\text{H}_2$  evolution from methanol/water solution with the  $\text{H}_2\text{PtCl}_6$  solution and  $\text{TiO}_2$  catalyst was evaluated using a glass tube. The light source was a DC 12 V LED (POT-365, Asahi Spectra Co., Japan). The catalyst (2.0 mg) and 53  $\mu\text{L}$  of  $\text{H}_2\text{PtCl}_6$  solution (0.02 mg Pt) were dispersed into an aqueous methanol solution (1 mL of  $\text{CH}_3\text{OH}$  and 4 mL of  $\text{H}_2\text{O}$ ) with magnetic stirring. The  $\text{H}_2$  yield was quantified by a gas chromatograph (GC-8A, Shimadzu Co., Japan) equipped with a thermal conductivity detector and Ar gas as the carrier.

### 2.5. Time-resolved diffuse reflectance spectral measurements

The TDR test was conducted by the pump and probe method using a regeneratively amplified titanium sapphire laser (Spectra-Physics, Spitfire Pro F, 1 kHz, Newport Inc., USA) pumped by a Nd:YLF laser (Spectra-Physics, Empower 15, Newport Inc., USA). The seed pulse was generated by a titanium sapphire laser (Spectra-Physics, Mai Tai VFSJW; fwhm 80 fs, Newport Inc., USA). The fourth harmonic generation (330 nm, 3  $\mu\text{J}$  pulse $^{-1}$ ) of the optical parametric amplifier (Spectra-Physics, OPA-800CF-1, Newport Inc., USA) was used as the excitation pulse. A white light continuum pulse generated by focusing the residual of the fundamental light on a sapphire crystal after the computer controlled optical delay, was divided into two parts and used as the probe and reference lights, of which the latter was used to compensate the laser fluctuation. Both probe and reference lights were directed to the sample powder coated on the glass substrate, and the reflected lights were detected by a linear InGaAs array detector equipped with the polychromator (Solar, MS3504, Newport Inc., USA). The pump pulse was chopped by the mechanical chopper synchronized to one-half of the laser repetition rate, resulting in a pair of spectra with and without the pump, from which the absorption change (% Abs) induced by the pump pulse was estimated. All measurements were carried out at ambient temperature around  $25^\circ\text{C}$ .

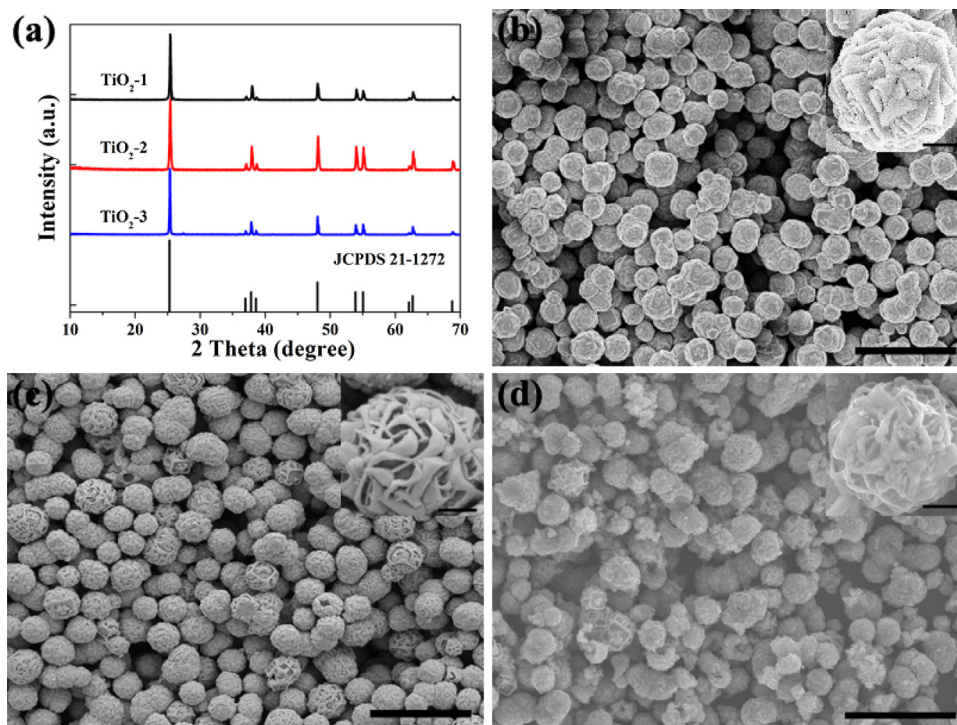


**Fig. 1.** (a) XRD patterns of the products; (b, c) SEM images of the products at different solvothermal reaction times (b)  $\text{TiO}_2$ -1 (4 h), (c)  $\text{TiO}_2$ -2 (12 h), and (d) SEM image of  $\text{TiO}_2$ -3 after annealing. The scale bars are 10  $\mu\text{m}$ , and insets are 1  $\mu\text{m}$ .

### 3. Results and discussion

#### 3.1. Structural, morphological and chemical characteristics of the $\text{TiO}_{2-x}$ microspheres

The XRD patterns of the three samples in Fig. 1a show similar diffraction peaks, indicating that the obtained samples were anatase  $\text{TiO}_2$  and no overlapping of this peak with any other peaks from other phases occurred, in agreement with the standard anatase (JCPDS No. 21-1272). The morphologies of the as-obtained anatase  $\text{TiO}_2$  microspheres with different solvothermal reaction times are shown in Fig. 1b and c. The spheres are uniform with an average size of  $\sim 3 \mu\text{m}$ . In the high magnification micrographs (insets of Fig. 1b and c), the constituent nanosheets and etching nanosheets are clearly observed. After etching, gaps and pores were formed on the self-assembly microsphere surface. As shown in Fig. 1d, the morphology of sample  $\text{TiO}_2$ -3 remains keeping the basic shape with forming small particles after annealing sample  $\text{TiO}_2$ -2. The XRD pattern, SEM images and energy-dispersive x-ray spectroscopies of Pt/ $\text{TiO}_2$ -2 sample are shown in Fig. S1.

To further explore the morphological development and formation mechanism of the three dimensional hierarchical structures of anatase  $\text{TiO}_2$  microspheres, more systematic experiments were carried out. Fig. 2 shows a schematic representation of the growth process of a microsphere, synthesized by solvothermal treatment at 433 K with different reaction times in a solution containing fluorine ions. From the SEM images of the serial samples, nanosheets and nanoparticles were produced in solution at the initial stage of the reaction (Fig. 2a). Then, the nanosheets and nanoparticles gathered to generate nanospheres (Fig. 2b), and finally the nanospheres continued growing to form microspheres with exposed major (101) and (001) facets (Fig. 2c, d) [20].

The SEM images of the products at different reaction times from 3 to 6 h (Fig. 2d–f) show that the etched anatase microspheres in Fig. 1c were developed from the selective etching of the anatase

$\text{TiO}_2$ , produced at the initial stage of the reaction (Fig. 2d). Due to the etching effect of the excess HF in the reaction, numerous pits were generated simultaneously at the joint among the anatase  $\text{TiO}_2$  nanosheets at the early stages. These pits were then enlarged gradually, and the center of the (001) facets almost disappeared by etching in the reaction. As a result, complex nanostructures were generated (Fig. 2f). Interestingly, when the reaction time was prolonged to 12 h, more complex structures with an entirely etching (001) facets morphology was obtained (inset of Fig. 1d). Such a formation process could be considered as the result of the continuous etching of the original structures [20,21]. In this process, HF has an etching effect on the (001)-faceted anatase  $\text{TiO}_2$  in the presence of water and the etching usually occurs on the (001)-faceted surfaces. Moreover, the degree of etching and the morphology of the resulting products vary remarkably by prolonging the reaction time.

The XPS analysis was used to probe the chemical state of Ti to gain more insight into the oxygen vacancies in the  $\text{TiO}_2$  samples. The XPS spectrum of Ti 2p shown in Fig. 3b exhibits two peaks at 458.6 and 464.3 eV with a spin–orbital doublet splitting ( $\text{Ti } 2p_{3/2}$ – $\text{Ti } 2p_{1/2}$ ) of 5.7 eV to be assigned to 4+ oxidation state of titanium as  $\text{Ti}^{4+}$  [22]. No peak corresponding to  $\text{Ti}^{3+}$  around 458.1 eV was detected. This result demonstrates that the surface of blue  $\text{TiO}_{2-x}$  was dominated by  $\text{Ti}^{4+}$ , ruling out the presence of  $\text{Ti}^{3+}$  on the sample surface, indicating that stoichiometric  $\text{TiO}_2$  microspheres were formed on the surface of non-stoichiometric  $\text{TiO}_{2-x}$  core-microcrystals [23]. The radius of the  $\text{TiO}_2$  microsphere was about 1.5  $\mu\text{m}$ , larger than the detection limit of XPS [13]. The  $\text{TiO}_{2-x}$  microspheres were much stable than the previously reported  $\text{TiO}_{2-x}$  NPs, prepared through  $\text{H}_2$ -reduction method and not stable due to the presence of oxygen vacancies on the surface of NPs [24].

The low temperature EPR was recorded at 130 K to identify the presence of  $\text{Ti}^{3+}$  in the  $\text{TiO}_{2-x}$  microspheres and the results are shown in Fig. 4. At this temperature, the anisotropic g tensors for the sample could not be resolved.  $\text{TiO}_2$ -2 had a very strong EPR signal

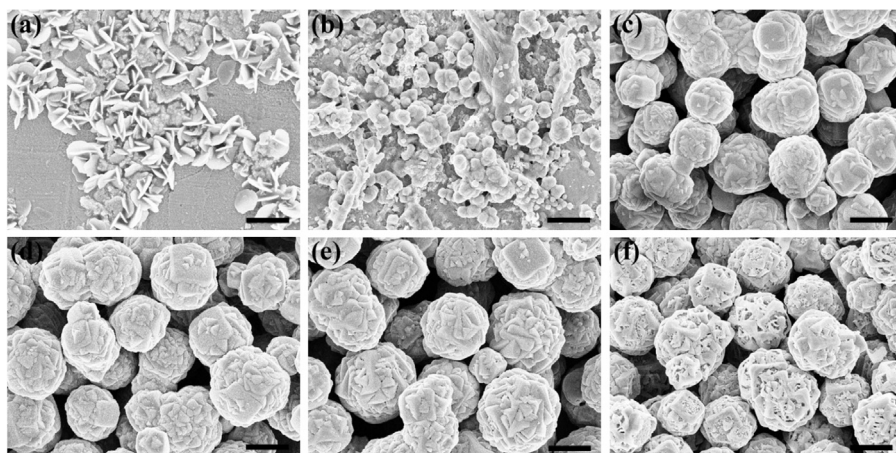


**Fig. 2.** SEM images of the products from the one-step solvothermal reaction at different reaction times (a) 1 h, (b) 1.5 h, (c) 2 h, (d) 3 h, (e) 4 h, and (f) 6 h. The scale bars are 2  $\mu\text{m}$ .

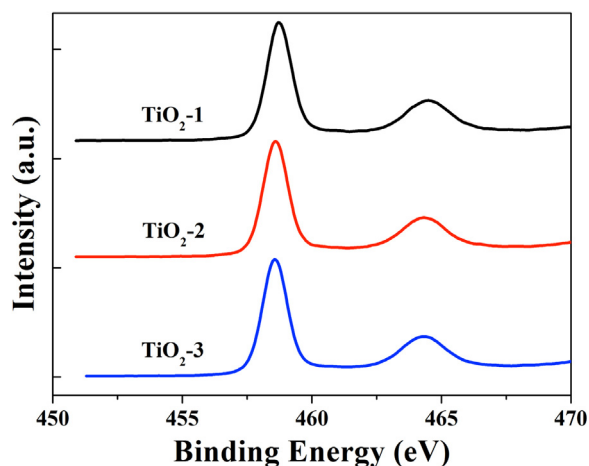


**Fig. 3.** XPS spectra of the obtained  $\text{TiO}_{2-x}$  microspheres: a high resolution characteristic peak of Ti 2p recorded from the pristine surface layer prepared at different solvothermal reaction times.

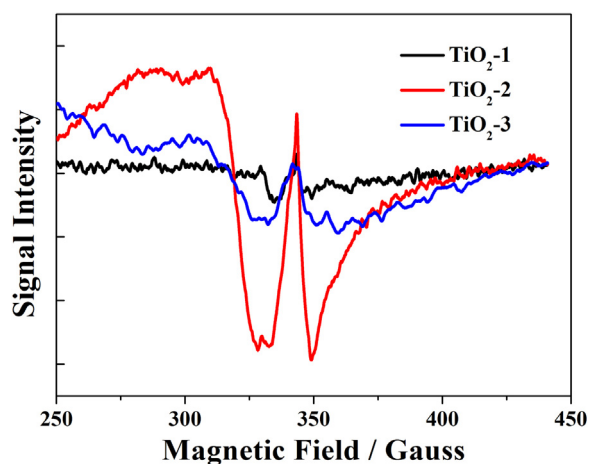


**Fig. 4.** The X-band EPR spectra of  $\text{Ti}^{3+}$  self-doped  $\text{TiO}_{2-x}$  microspheres samples  $\text{TiO}_{2-1}$ ,  $\text{TiO}_{2-2}$  and  $\text{TiO}_{2-3}$  recorded at  $T = 130\text{ K}$ .

at  $g = 1.97$  to be attributed to subsurface paramagnetic  $\text{Ti}^{3+}$  centers [25,26]. Weak signals were seen for  $\text{TiO}_{2-1}$  and  $\text{TiO}_{2-3}$ , indicating that a great amount of  $\text{Ti}^{3+}$  was produced in the  $\text{TiO}_{2-x}$  microspheres by prolonging the solvothermal reaction time or annealing sample

in air. In the annealing progress,  $\text{Ti}^{3+}$  can be oxidated to generate  $\text{Ti}^{4+}$  in air and the oxygen vacancy should decrease [27,28].

The EPR spectra also exclude the presence of  $\text{Ti}^{3+}$  on the sample surface. Since the surface  $\text{Ti}^{3+}$  is prone to adsorb atmospheric  $\text{O}_2$ , which would be reduced to  $\text{O}_2^-$  and show an EPR signal at  $g = 2.02$  [29]. However, no EPR signal at  $g = 2.02$  was observed.

The microstructures of the etching microspheres were further examined by using TEM (Fig. 5a, b), high-resolution TEM (Fig. 5c), and selected-area electron diffraction (SAED) (inset of Fig. 5c). The TEM image in Fig. 5a shows that the obtained  $\text{TiO}_{2-x}$  microspheres had a uniform average size of ca. 3  $\mu\text{m}$ , corresponding to the SEM (Fig. 2) and the microstructure image of a representative microsphere respectively. The distinguished one-dimensional lattice fringes in Fig. 5c indicate that the obtained etching  $\text{TiO}_{2-x}$  microspheres were well crystallized with a lattice fringe spacing of 0.36 nm (measured by Digital Micrograph in Fig. 5d), corresponding to the (101) facets of anatase  $\text{TiO}_2$ . More importantly, it provides direct evidence that (001) facets were etched and (101) facets remained. This is in agreement with the above analysis of the morphological development and formation mechanism.

Compared with etching and non-etching  $\text{TiO}_2$ , the BET surface area is also important for photocatalytic activity. As shown in Fig. 6, the obtained samples had normalized BET surface areas of 2.7 ( $\text{TiO}_{2-1}$ ), 3.2 ( $\text{TiO}_{2-2}$ ), and 2.5 ( $\text{TiO}_{2-3}$ )  $\text{m}^2/\text{g}$  from nitrogen adsorption-desorption isotherm plots, respectively. There was a small difference in BET surface area for the three samples.

### 3.2. Optical and photoelectrochemical properties of the $\text{TiO}_{2-x}$ microspheres

The optical response of  $\text{Ti}^{3+}$  self-doped  $\text{TiO}_{2-x}$  microspheres samples is shown in Fig. 7 with a comparison to that of other samples. For the  $\text{Ti}^{3+}$  self-doped  $\text{TiO}_{2-x}$  microspheres (Fig. 7, red ( $\text{TiO}_{2-2}$ )), a considerably large absorption tail in the visible regions was observed, in consistent with the change in color of the powder solution (inset in Fig. 7). This gives clear evidence that the non-stoichiometric  $\text{TiO}_{2-x}$  microspheres contained a large number of oxygen vacancies [23]. These results indicate that the  $\text{Ti}^{3+}$ -induced visible-light absorption is formed as isolated states between the forbidden gap in  $\text{TiO}_2$ , as reported previously [13]. Theoretical studies also demonstrated that  $\text{Ti}^{3+}$  inside the bulk  $\text{TiO}_2$  and the high oxygen vacancy concentration could form an electronic state vacancy band below the conduction band, which is responsible for the band-gap narrowing [25].

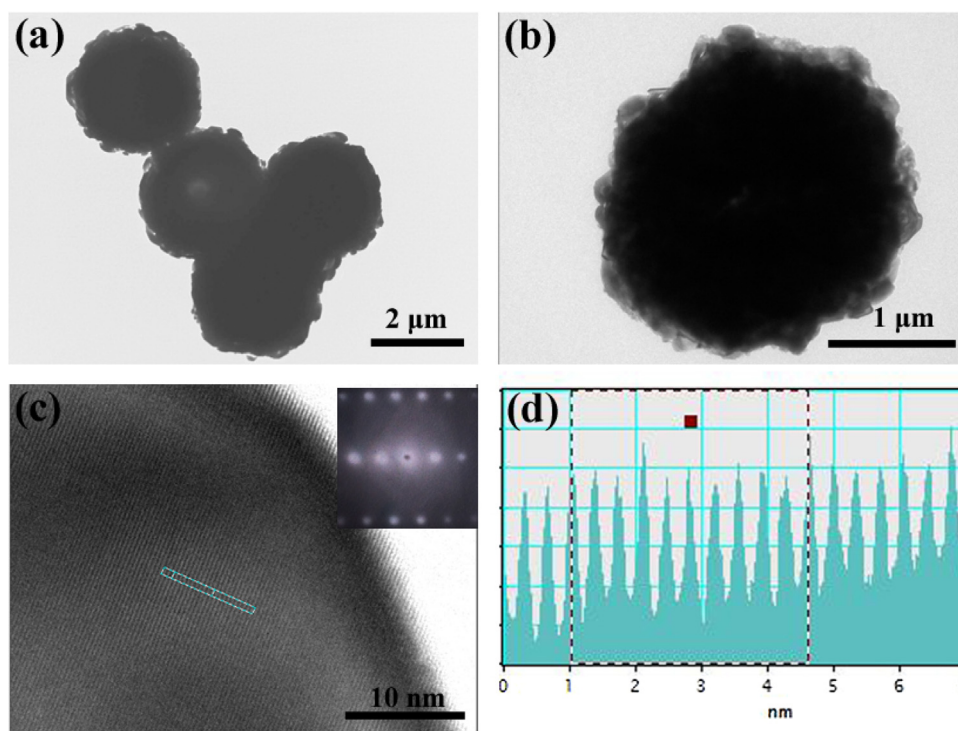


**Fig. 5.** Structural characteristics of the as-prepared  $\text{Ti}^{3+}$  self-doped  $\text{TiO}_{2-x}$  sample ( $\text{TiO}_2$ -2) after 12-h solvothermal reaction at  $160^\circ\text{C}$ : (a) Typical TEM images of several microspheres; (b) Magnified TEM image of a single representative microsphere; (c) HRTEM image of the etched surface from a microsphere, and SAED pattern (inset) showing single-crystal diffraction; and (d) Digital micrograph.

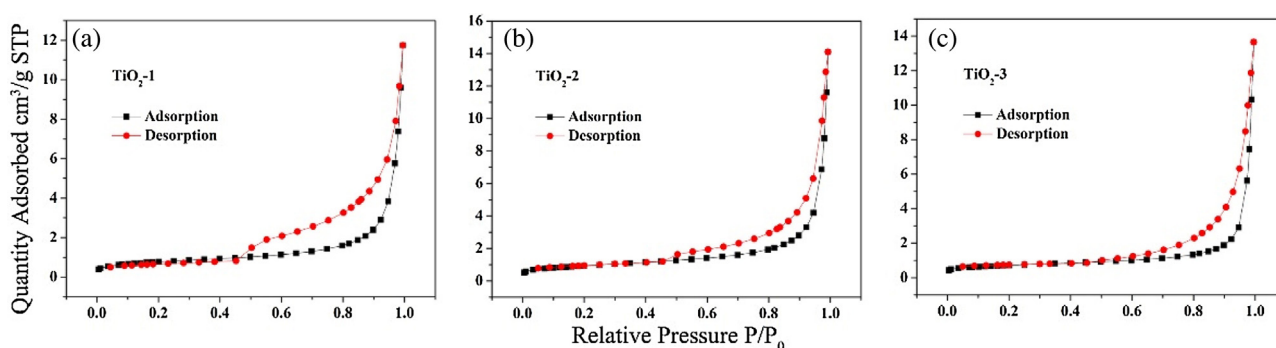


**Fig. 6.** Nitrogen adsorption-desorption isotherm plot of the as-prepared  $\text{TiO}_2$  samples.

The responsive photocurrent intensity of the obtained samples under UV irradiation can reflect the overall photoelectron-conversion process (Fig. 8a) [30]. The photocurrent on  $\text{TiO}_2$ -2 was nearly 2 and 6 times higher than those on  $\text{TiO}_2$ -3 and  $\text{TiO}_2$ -1, respectively. This revealed that the  $\text{Ti}^{3+}$  self-doped  $\text{TiO}_2$  with designed (101) facet was beneficial for photoinduced charge separation and transport.

Correspondingly, EIS result can provide additional information and better understanding on the interfacial reactions of photoexcited electrons in photocatalysis [30]. Fig. 8b shows the EIS spectra of the photocatalysis using  $\text{TiO}_2$ -1,  $\text{TiO}_2$ -2, and  $\text{TiO}_2$ -3 respectively. The measured smaller arc radius on the  $\text{TiO}_2$ -2 electrode clearly exhibited an enhanced electrochemical conductivity, reduced electron transfer resistance, and magnified separation and transfer ability of electro-generated carriers [31], compared to the other samples (Fig. 8b).

### 3.3. Photocatalytic $\text{H}_2$ evolution over the $\text{TiO}_{2-x}$ microspheres

The photocatalytic  $\text{H}_2$  evolution from water/methanol (4:1 mL) by the  $\text{TiO}_2$  catalysts (deposited with Pt as cocatalyst 1 wt%) was investigated. Fig. 9 shows that the  $\text{H}_2$  evolution rate was elevated by facet etching and  $\text{Ti}^{3+}$  self-doping. On one hand, the photocatalytic  $\text{H}_2$  evolution of  $\text{TiO}_2$ -3 with (001) facet etching was 2.6 times higher than that for  $\text{TiO}_2$ -1. (001) and (101) facets are oxidation and reduction facets, respectively. Thus, the predominated presence of reductive (101) facet is beneficial for photocatalytic  $\text{H}_2$  evolution. On the other hand, photocatalytic  $\text{H}_2$  evolution of  $\text{TiO}_2$ -2 was 1.3 times higher than that for  $\text{TiO}_2$ -3, demonstrating that the changed electronic structure induced by  $\text{Ti}^{3+}$  self-doping lead to the enhanced  $\text{h}^+/\text{e}^-$  separation and increased photocatalytic  $\text{H}_2$  evolution. In this case, both  $\text{Ti}^{3+}$  self-doping and facet etching played important roles in charge separation and electron transfer [10]. Because of the small difference of BET for the samples ( $\text{TiO}_2$ -1, 2 and 3), their capability of  $\text{H}_2$  evolution per unit surface area should be examined. The

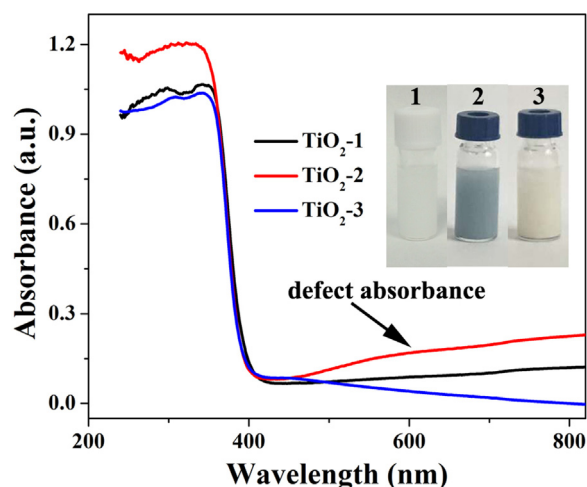


**Fig. 7.** UV-vis diffuse reflectance spectra of the as-prepared samples. The inset is the corresponding photographs.

normalized  $H_2$  evolution capacities of the Pt-loaded samples were 116, 334, and  $326 \mu\text{mol}/(\text{h m}^2)$ , respectively. This result also indicates that facet-etching played an important role in photocatalytic activity, but the effects of both BET surface and  $\text{Ti}^{3+}$ -doping photocatalytic activity are limited. From the repeated runs of  $H_2$  evolution (Fig. S3), the Pt/TiO<sub>2</sub>-2 sample exhibited a good stability. Moreover, the EPR spectra of the Pt/TiO<sub>2</sub>-2 sample were similar to those of the TiO<sub>2</sub>-2 sample (Fig. S4). This result indicates that the TiO<sub>2</sub>-2 sample was stable after the photocatalytic reaction.

#### 3.4. Charge transfer dynamics and reaction mechanism on the TiO<sub>2-x</sub> microspheres

As a powerful technique [32], the femtosecond TDR spectroscopic measurement was performed to clarify the charge carrier dynamics in the photocatalytic reaction under UV light irradiation (Fig. 10). After 330 nm laser excitation of TiO<sub>2</sub>-2 in ambient air (Fig. 10b), a broad absorption band appeared in the near-infrared region, which was superimposed with trapped and free electrons in TiO<sub>2</sub>-2. Similar absorption spectra were observed for TiO<sub>2</sub>-1 and TiO<sub>2</sub>-3 (Fig. 10a, c). During the period of 0–10 ps, the transient absorption of TiO<sub>2</sub>-2 decayed rapidly when compared with TiO<sub>2</sub>-1 and TiO<sub>2</sub>-3 (Fig. 10d). After the sufficient generation of charge carriers upon the 330-nm laser excitation of TiO<sub>2</sub>-1 and TiO<sub>2</sub>-3, electrons were excited from valance band O 1s to the conduction band Ti 3d to be directly trapped ( $\tau_1 = 6.1$  and 6.4 ps, respectively;

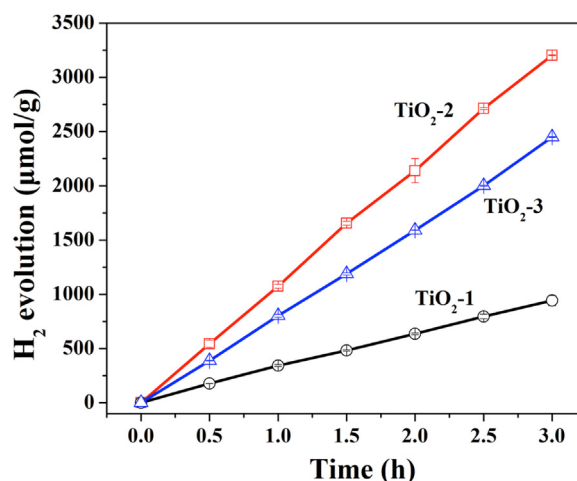


**Fig. 9.** Time course of evolved  $H_2$  under UV irradiation ( $70 \text{ mW}/\text{cm}^2$ , 365-nm LED) by the TiO<sub>2</sub> catalysts.

**Table 1**

Kinetic parameters of decays for TiO<sub>2</sub> catalysts under the UV laser excitation.

Sample	UV laser (330 nm, $3 \mu\text{J pulse}^{-1}$ )		
	$\tau_1$ (ps)	$\tau_2$ (ps)	$\tau_3$ (ps)
TiO <sub>2</sub> -1	6.1	41	471
TiO <sub>2</sub> -2	3.8	33	342
TiO <sub>2</sub> -3	6.4	62	532

Table 1). On the other hand, the generated holes were separated and localized at the O 1s state valance band at the same time [33]. After the equilibrium between electrons in the surface trap and the bulk ( $\tau_2 = 41$  and 62 ps, respectively; Table 1), the favorable reduction pathway and charge recombination occurred ( $\tau_3 = 472$  and 532 ps, respectively; Table 1) in TiO<sub>2</sub>-1 and TiO<sub>2</sub>-3. Therefore, TiO<sub>2</sub>-3 with a higher efficiency exhibited a longer lifetime of two components ( $\tau_2 = 62$  ps and  $\tau_3 = 532$  ps) than those for TiO<sub>2</sub>-1, exhibiting the similar photocatalytic efficiency under the UV irradiation. However, it is unusual that TiO<sub>2</sub>-2 with a higher efficiency exhibited a shorter lifetime of the components ( $\tau_2 = 33$  ps and  $\tau_3 = 342$  ps) than both TiO<sub>2</sub>-1 and TiO<sub>2</sub>-3. It might be attributed to the fact that  $\text{Ti}^{3+}$  served as a midgap state and captured the position of carriers [13]. As a result, the shorter lifetime of TiO<sub>2</sub>-2 ( $\tau_1 = 3.8$  ps) observed at the first decay component corresponded to  $\text{Ti}^{3+}$  at midgap state compared with TiO<sub>2</sub>-1 and TiO<sub>2</sub>-3. Then, TiO<sub>2</sub>-2 achieved the equilibrium between electrons in the surface trap and

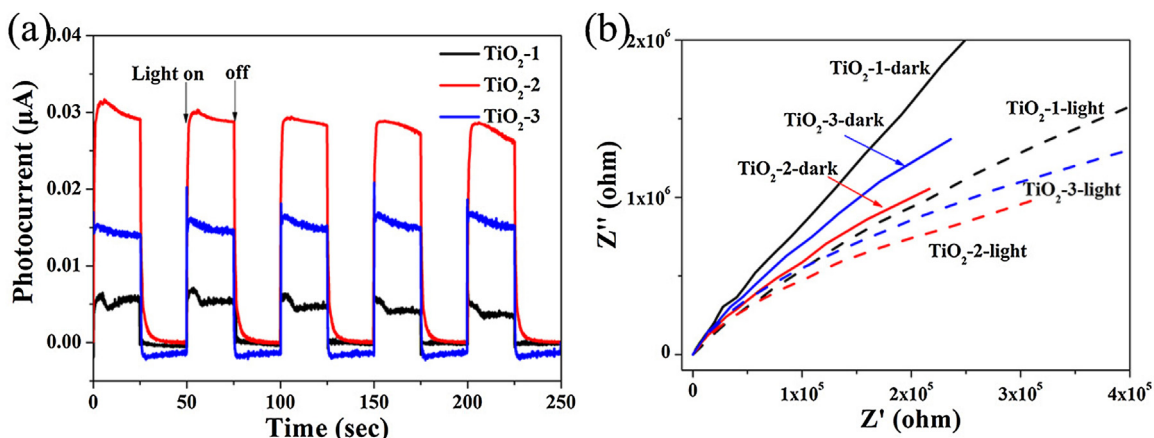


**Fig. 8.** Photocurrent versus time plots (a) and EIS Nyquist plots (b) of the obtained samples.

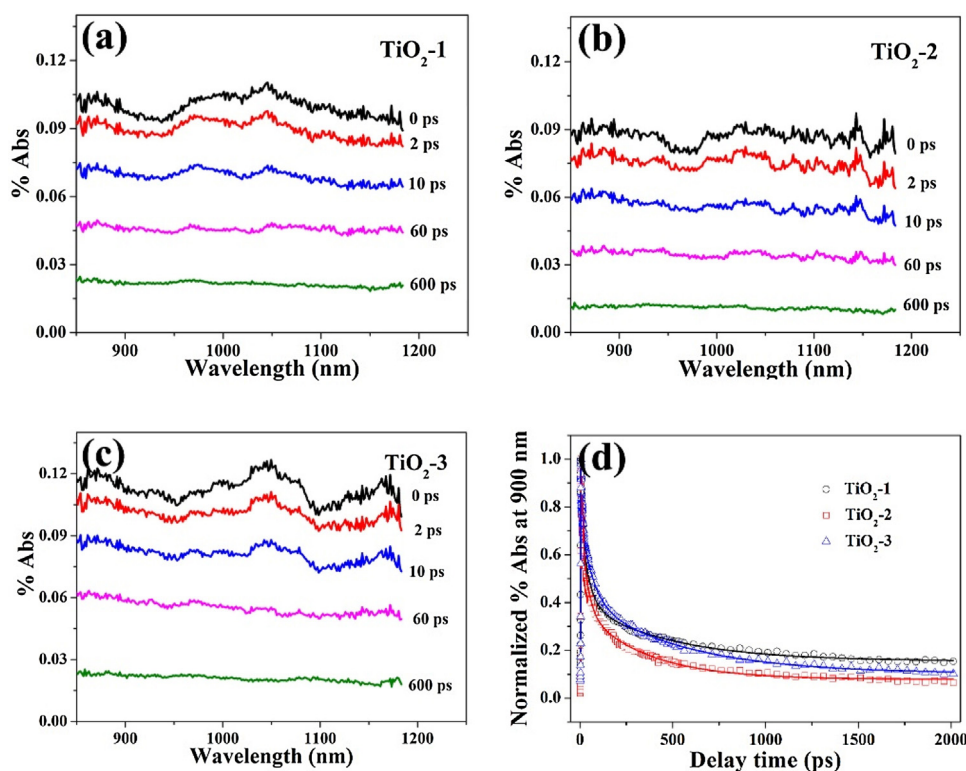


**Fig. 10.** The TDR spectra of the obtained samples (a)  $\text{TiO}_2$ -1, (b)  $\text{TiO}_2$ -2, and (c)  $\text{TiO}_2$ -3. (d) Normalized transient absorption traces observed at 900 nm for a range of samples.

the bulk immediately ( $\tau_2 = 33$  ps), and the favorable reduction pathway and charge recombination occurred more rapidly ( $\tau_3 = 342$  ps) [34].

#### 4. Conclusions

In summary, nonstoichiometric  $\text{TiO}_2$  with desired (101) facets  $\text{TiO}_{2-x}$  microspheres was synthesized using a one-step solvothermal method. The obtained nonstoichiometric  $\text{TiO}_2$  with designed (101) facets ( $\text{TiO}_2$ -2) exhibited the highest photocatalytic  $\text{H}_2$  evolution (1.3 and 3.4 times higher those of  $\text{TiO}_2$ -3 and  $\text{TiO}_2$ -1, respectively). Experimental results show the presence of bulk  $\text{Ti}^{3+}$  defects generates mid gap electronic states within the band gap of  $\text{TiO}_2$  microspheres, and significantly improve the efficiency of electron-hole separation, thus greatly enhance the photocatalytic activity and  $\text{H}_2$  production. Moreover, the etching (101) facet in the  $\text{TiO}_2$  microspheres was also beneficial for electron-hole separation and transfer and accordingly the  $\text{H}_2$  evolution. This work provides a simple but efficient approach to prepare the  $\text{TiO}_2$  with simultaneous facet-etching and self-doping. Our findings open up a new avenue for efficient hydrogen generation based on the earth-abundant, scalable  $\text{TiO}_2$  catalysts, and may have implications in the optimization of other transition metal oxide electrocatalysts for energy conversion systems.

#### Acknowledgements

We thank the National Science Foundation of China (21261160489, 21590812 and 51538011) and the Collaborative Innovation Center of Suzhou Nano Science and Technology of the Ministry of Education of China, and a Grant-in-Aid for Scientific Research (Project 25220806 and others) from the Ministry of Education, Culture, Sports, Science and Technology (MEXT) of the Japanese Government, for support of this work.

#### Appendix A. Supplementary data

Supplementary data associated with this article can be found, in the online version, at <http://dx.doi.org/10.1016/j.apcatb.2016.12.036>.

#### References

- [1] Y. Ma, X.L. Wang, Y.S. Jia, X.B. Chen, H.X. Han, C. Li, Titanium dioxide-based nanomaterials for photocatalytic fuel generations, *Chem. Rev.* 114 (2014) 9987–10043.
- [2] A. Fujishima, K. Honda, Electrochemical photolysis of water at a semiconductor electrode, *Nature* 238 (1972) 37–38.
- [3] L. Liu, X.B. Chen, Titanium dioxide nanomaterials: self-structural modifications, *Chem. Rev.* 114 (2014) 9890–9918.
- [4] G. Liu, H.G. Yang, J. Pan, Y.Q. Yang, G.Q. Lu, H.M. Cheng, Titanium dioxide crystals with tailored facets, *Chem. Rev.* 114 (2014) 9559–9612.
- [5] W.K. Wang, J.J. Chen, X. Zhang, Y.X. Huang, W.W. Li, H.Q. Yu, Self-induced synthesis of phase-junction  $\text{TiO}_2$  with a tailored rutile to anatase ratio below phase transition temperature, *Sci. Rep.* 6 (2016) 20491.
- [6] S.K. Wallace, K.P. McKenna, Facet-dependent electron trapping in  $\text{TiO}_2$  nanocrystals, *J. Phys. Chem. C* 119 (2015) 1913–1920.
- [7] S. Selcuk, A. Selloni, Facet-dependent trapping and dynamics of excess electrons at anatase  $\text{TiO}_2$  surfaces and aqueous interfaces, *Nat. Mater.* 15 (2016) 1107–1112.
- [8] J.G. Yu, J.X. Low, W. Xiao, P. Zhou, M. Jaroniec, Enhanced photocatalytic  $\text{CO}_2$ -reduction activity of anatase  $\text{TiO}_2$  by coexposed {001} and {101} facets, *J. Am. Chem. Soc.* 136 (2014) 8839–8842.
- [9] T. Tachikawa, S. Yamashita, T. Majima, Evidence for crystal-face-dependent  $\text{TiO}_2$  photocatalysis from single-molecule imaging and kinetic analysis, *J. Am. Chem. Soc.* 133 (2011) 7197–7204.
- [10] X.G. Liu, G.J. Dong, S.P. Li, G.X. Lu, Y.P. Bi, Direct observation of charge separation on anatase  $\text{TiO}_2$  crystals with selectively etched {001} facets, *J. Am. Chem. Soc.* 138 (2016) 2917–2920.
- [11] J. Pan, G. Liu, G.M. Lu, H.M. Cheng, On the true photoreactivity order of {001}, {010}, and {101} facets of anatase  $\text{TiO}_2$  crystals, *Angew. Chem. Int. Ed.* 50 (2011) 2133–2137.
- [12] N.Q. Wu, J. Wang, D. Tafen, H. Wang, J.G. Zheng, J.P. Lewis, X.G. Liu, S.S. Leonard, A. Manivannan, Shape-enhanced photocatalytic activity of single-crystalline anatase  $\text{TiO}_2$  (101) nanobelts, *J. Am. Chem. Soc.* 132 (2010) 6679–6685.

- [13] Q. Zhu, Y. Peng, L. Lin, C.M. Fan, G.Q. Gao, R.X. Wang, A.W. Xu, Stable blue  $\text{TiO}_{2-x}$  nanoparticles for efficient visible light photocatalysts, *J. Mater. Chem. A* 2 (2014) 4429–4437.
- [14] Z.K. Zheng, B.B. Huang, X.D. Meng, J.P. Wang, S.Y. Wang, Z.Z. Lou, Z.Y. Wang, X.Y. Qin, X.Y. Zhang, Y. Dai, Metallic zinc-assisted synthesis of  $\text{Ti}^{3+}$  self-doped  $\text{TiO}_2$  with tunable phase composition and visible-light photocatalytic activity, *Chem. Commun.* 49 (2013) 868–870.
- [15] I. Nakamura, N. Negishi, S. Kutsuna, T. Ihara, S. Sugihara, E. Takeuchi, Role of oxygen vacancy in the plasma-treated  $\text{TiO}_2$  photocatalyst with visible light activity for NO removal, *J. Mol. Catal. A-Chem.* 161 (2000) 205–212.
- [16] T. Lemerrier, J.M. Mariot, P. Parent, M.F. Fontaine, C.F. Hague, M. Querton, Formation of  $\text{Ti}^{3+}$  ions at the surface of laser-irradiated rutile, *Appl. Surf. Sci.* 86 (1995) 382–386.
- [17] S. Hashimoto, A. Tanaka, Alteration of Ti 2p XPS spectrum for titanium oxide by low-energy Ar ion bombardment, *Surf. Interface Anal.* 34 (2002) 262–265.
- [18] W.K. Wang, J.J. Chen, M. Gao, Y.X. Huang, X. Zhang, H.Q. Yu, Photocatalytic degradation of atrazine by boron-doped  $\text{TiO}_2$  with a tunable rutile/anatase ratio, *Appl. Catal. B-Environ.* 195 (2016) 69–76.
- [19] W.K. Wang, J.J. Chen, W.W. Li, D.N. Pei, X. Zhang, H.Q. Yu, Synthesis of Pt-loaded self-interpersed anatase  $\text{TiO}_2$  with a large fraction of (001) facets for efficient photocatalytic nitrobenzene degradation, *ACS Appl. Mater. Interfaces* 7 (2015) 20349–20359.
- [20] X.H. Yang, H.G. Yang, C.Z. Li, Controllable nanocarving of anatase  $\text{TiO}_2$  single crystals with reactive {001} facets, *Chem.-Eur. J.* 17 (2011) 6615–6619.
- [21] W.Q. Fang, J.Z. Zhou, J. Liu, Z.G. Chen, C. Yang, C.H. Sun, G.R. Qian, J. Zou, S.Z. Qiao, H.G. Yang, Hierarchical structures of single-crystalline anatase  $\text{TiO}_2$  nanosheets dominated by {001} facets, *Chem.-Eur. J.* 17 (2011) 1423–1427.
- [22] J.G. Li, R. Buechel, M. Isobe, T. Mori, T. Ishigaki, Cobalt-doped  $\text{TiO}_2$  nanocrystallites: radio-frequency thermal plasma processing, phase structure, and magnetic properties, *J. Phys. Chem. C* 113 (2009) 8009–8015.
- [23] F. Zuo, K. Bozhilov, R.J. Dillon, L. Wang, P. Smith, X. Zhao, C. Bardeen, P.Y. Feng, Active facets on titanium(III)-doped  $\text{TiO}_2$ : an effective strategy to improve the visible-light photocatalytic activity, *Angew. Chem. Int. Ed.* 51 (2012) 6227–6230.
- [24] M.Y. Xing, J.L. Zhang, F. Chen, B.Z. Tian, An economic method to prepare vacuum activated photocatalysts with high photo-activities and photosensitivities, *Chem. Commun.* 47 (2011) 4947–4949.
- [25] F. Zuo, L. Wang, T. Wu, Z.Y. Zhang, D. Borchardt, P.Y. Feng, Self-Doped  $\text{Ti}^{3+}$  enhanced photocatalyst for hydrogen production under visible light, *J. Am. Chem. Soc.* 132 (2010) 11856–11857.
- [26] Q. Chen, W. Ma, C. Chen, H. Ji, J. Zhao, Anatase  $\text{TiO}_2$  mesocrystals enclosed by (001) and (101) facets: synergistic effects between  $\text{Ti}^{3+}$  and facets for their photocatalytic performance, *Chem.-Eur. J.* 18 (2012) 12584–12589.
- [27] Y.F. Ji, W. Guo, H.H. Chen, L.S. Zhang, S. Chen, M.T. Hua, Y.H. Long, Z. Chen, Surface  $\text{Ti}^{3+}/\text{Ti}^{4+}$  redox shuttle enhancing photocatalytic  $\text{H}_2$  production in ultrathin  $\text{TiO}_2$  nanosheets/CdSe quantum dots, *J. Phys. Chem. C* 119 (2015), 27063–27059.
- [28] Y.M. Liu, J.P. Wang, P. Yang, K. Matras-Postolek, Self-modification of  $\text{TiO}_2$  one-dimensional nano-materials by  $\text{Ti}^{3+}$  and oxygen vacancy using  $\text{Ti}_2\text{O}_3$  as precursor, *RSC Adv.* 5 (2015) 61657–61663.
- [29] X.X. Zou, J.K. Liu, J. Su, F. Zuo, J.S. Chen, P.Y. Feng, Facile synthesis of thermal- and photostable titania with paramagnetic oxygen vacancies for visible-light photocatalysis, *Chem.-Eur. J.* 19 (2013) 2866–2873.
- [30] Y. Hou, F. Zuo, A. Dagg, P.Y. Feng, A three-Dimensional branched cobalt-doped  $\alpha\text{-Fe}_2\text{O}_3$  Nanorod/ $\text{MgFe}_2\text{O}_4$  heterojunction array as a flexible photoanode for efficient photoelectrochemical water oxidation, *Angew. Chem. Int. Edit.* 52 (2013) 1248–1252.
- [31] Z. Hosseini, N. Taghavinia, N. Sharifia, M. Rahmana, F. Tajabadib, Evaluation of a High Conductivity  $\text{TiO}_2/\text{Ag}$  Fibrous Electrode with EIS Measurements, *Rct* ( $\Omega$ ) 2500, 1260.
- [32] P. Zhang, M. Fujitsuka, T. Majima,  $\text{TiO}_2$  mesocrystal with nitrogen and fluorine codoping during topochemical transformation: efficient visible light induced photocatalyst with the codopants, *Appl. Catal. B-Environ.* 185 (2016) 181–188.
- [33] J. Schneider, M. Matsuoka, M. Takeuchi, J.L. Zhang, Y. Horiuchi, M. Anpo, D.W. Bahnemann, Understanding  $\text{TiO}_2$  photocatalysis: mechanisms and materials, *Chem. Rev.* 114 (2014) 9919–9986.
- [34] P. Zhang, T. Tachikawa, M. Fujitsuka, T. Majima, Atomic layer deposition-confined nonstoichiometric  $\text{TiO}_2$  nanocrystals with tunneling effects for solar driven hydrogen evolution, *J. Phys. Chem. Lett.* 7 (2016) 1173–1179.